

Chiral 1D Floquet topological insulators beyond rotating wave approximation

Dante M. Kennes,¹ Niclas Müller,² Mikhail Pletyukhov,² Clara Weber,² Christoph Bruder,³ Fabian Hassler,⁴ Jelena Klinovaja,³ Daniel Loss,³ and Herbert Schoeller^{2,*}

¹*Dahlem Center for Complex Quantum Systems and Fachbereich Physik, Freie Universität Berlin, 14195 Berlin, Germany*

²*Institut für Theorie der Statistischen Physik, RWTH Aachen, 52056 Aachen, Germany and JARA - Fundamentals of Future Information Technology*

³*Department of Physics, University of Basel, Klingelbergstrasse 82, CH-4056 Basel, Switzerland*

⁴*JARA-Institute Quantum Information, RWTH Aachen University, 52056 Aachen, Germany*

(Dated: May 14, 2020)

We study one-dimensional (1D) Floquet topological insulators with chiral symmetry going beyond the standard rotating wave approximation. The occurrence of many anticrossings between Floquet replicas leads to a dramatic extension of phase diagram regions with stable topological edge states (TESs). We present an explicit construction of all TESs in terms of a truncated Floquet Hamiltonian in frequency space, prove the bulk-boundary correspondence, and analyze the stability of the TESs in terms of their localization lengths. We propose experimental tests of our predictions in curved bilayer graphene.

The search for materials in which topologically protected edge states can be induced and controlled has led to much research attention in the field of Floquet topological insulators (FTIs) in the last decade. In FTIs topology is induced by external driving which implies an intriguing degree of tunability. These systems were classified [1-12] and first experimental tests were discussed in photonic crystals [13-18], cold atom systems [19-21], and solid state materials [22-28]. Many promising proposals were made for realizing, e.g., Majorana edge modes [29-33] and parafermions [34] in 1D FTIs, the photo-induced quantum Hall effect in 2D materials [35-39], topological surface states in 3D FTIs [40], and Weyl semimetals and fractional FTIs in coupled Rashba nanowires [41].

A particular feature of FTIs distinguishing them fundamentally from static TIs is the fact that the driving frequency ω leads to an infinite set of Floquet replicas defined by shifting the conduction and valence band by $n\omega$ [42] corresponding to absorption/emission of n photons. This leads to a hierarchy of Floquet-induced anticrossings in the center of the bulk gap, which occurs for all solid state realizations of FTIs where the band width W is typically large compared to ω . This property has received only little attention so far. Previous works considered either the case of large driving frequency $\omega \gtrsim W$, where all Floquet bands are clearly separated, or the case of small driving amplitude $t_F \ll \omega$, where the hierarchy of anticrossings can either be treated perturbatively in t_F [39] or one can use the rotating wave approximation (RWA) [34, 37, 40, 41]. In RWA one tunes ω in resonance with the gap Δ_g between the conduction and valence band such that only the conduction band and the first replica of the valence band are relevant. The perturbative regime of very small frequencies $\omega \ll \Delta_g$ has been treated in Refs. 43-45.

In this Letter we consider solid state applications of FTIs in the generic regime, where all energy scales

t_F, ω, Δ_g are of comparable order and much smaller than W . In this regime, all Floquet replica-bands are strongly coupled and perturbative approaches are not applicable. We will concentrate on the case of 1D systems with chiral symmetry of the BDI class, however, our results have more general implications [46, 47]. As a testbed, we study the driven 2-band Rashba nanowire in a Zeeman field Δ_Z proposed in Ref. 34, which, e.g., can be realized in curved bilayer graphene, where the band gap and the Rashba spin-orbit interaction (SOI) are tunable [48]. For the BDI class, the topological invariant is a winding number where an arbitrary positive number of TESs can be realized. By tuning t_F and Δ_Z , we will show that FTIs offer the possibility to access many of these topological phases. Most importantly, we find many regions in the phase diagram where several coexisting TESs appear of which some are strongly localized with localization length comparable to the one appearing in the RWA phase. These TESs are stable and expected to be observable in experiments. As a consequence, compared to static TIs and FTIs in the RWA regime, we find a dramatic extension of possible topological phase diagram regions. This strongly motivates experimental tests of the physics of FTIs at large driving amplitude in solid state systems and implies novel opportunities to detect unambiguous fingerprints of topological states.

To efficiently deal with the intriguing problem of strongly coupled Floquet bands, we propose an analysis based on the truncated Floquet Hamiltonian in frequency space. The strongly localized TES of interest appear already in low truncation order and convergence is reached rapidly even for large driving amplitude. Furthermore, in the presence of chiral symmetry, we show that the number of boundary conditions can be reduced, in such a way that the number of TESs can be related straightforwardly to the number of roots of the determinant of the off-diagonal blocks of the Floquet Hamiltonian in the chi-

ral basis as a function of complex quasimomentum. This allows for an elegant formulation of the bulk-boundary correspondence together with the determination of the localization length of all TESs.

Model— As a testbed we will use a tight-binding version of a recently proposed 2-band Rashba nanowire where TESs appear when tuning a transverse Zeeman splitting Δ_Z or a driving field t_F , coupling the conduction and valence band [34]. The bulk Hamiltonian in quasimomentum space is given by $\tilde{h}_k(t) = (E_k + \frac{\Delta_g}{2} + \alpha_k \sigma_z) \eta_z + \Delta_Z \sigma_x + 2t_F \cos(\omega t) \eta_x$, with quasimomentum $-\pi < k \leq \pi$, dispersion relation $E_k = W \sin^2(k/2)$, and Rashba SOI $\alpha_k = \alpha \sin k$. Here, σ_i and η_i are Pauli matrices describing the spin and band degrees of freedom, respectively. At resonance $\Delta_g = \omega$, we transform to the RWA basis by using the unitary transformation $U(t) = \frac{1}{2} \sum_{\pm} (1 \pm \eta_z) e^{\mp i \omega t / 2}$. The transformed Hamiltonian is given by

$$h_k(t) = h_k^R + t_F (\eta_+ e^{i\Omega t} + \eta_- e^{-i\Omega t}), \quad (1)$$

with $\eta_{\pm} = \frac{1}{2}(\eta_x \pm i\eta_y)$ and an effective driving frequency $\Omega = 2\omega$. Here, $h_k^R = (E_k + \alpha_k \sigma_z) \eta_z + \Delta_Z \sigma_x + t_F \eta_x$ is the bulk Hamiltonian in RWA [34]. It leads to a TES at zero energy for $t_F < \Delta_Z$ similar to the Majorana model proposed in Ref. 49. However, beyond RWA, the second term on the r.h.s. of Eq. (1) is an important correction term which can change the phase diagram significantly for larger values of $t_F, \Delta_Z \sim \Omega$.

Truncated Floquet Hamiltonian in frequency space— The model defined by Eq. (1) falls into the class of generic time-periodic 1D systems with local chiral symmetry $S h_k(t) S = -h_k(-t)$, where $S = \sigma_z \eta_y$ for our specific case. The Floquet Hamiltonian is defined by $(h_k^F)_{ll'} = h_{k,l-l'} - l \Omega \delta_{ll'}$, where $l = 0, \pm 1, \pm 2, \dots$ denotes the Floquet modes and $h_{k,l} = \frac{1}{T} \int_0^T dt e^{i l \Omega t} h_k(t)$ with $T = \frac{2\pi}{\Omega}$. It has a chiral symmetry $S_o h_k^F S_o = -h_k^F$ w.r.t. zero energy, with $S_o = SP$ and $P|l\rangle = |-l\rangle$. Since the Floquet spectrum is defined modulo Ω , there is also a chiral symmetry $S_e (h_k^F + \frac{\Omega}{2}) S_e = -(h_k^F + \frac{\Omega}{2})$ w.r.t. energy $-\frac{\Omega}{2}$, with $S_e = ST_1 P$ and $T_1|l\rangle = |l+1\rangle$. At $E = -\frac{\Omega}{2}, 0$ (modulo Ω), two gaps open up due to the couplings Δ_Z and t_F . We are interested in TESs with a localization length up to a certain threshold at these two energies. To analyze their occurrence, we truncate h_k^F by an even (odd) number $2l_{\max}$ ($2l_{\max} + 1$) of Floquet replicas, where $l = -l_{\max} + 1, \dots, l_{\max}$ ($l = -l_{\max}, \dots, l_{\max}$) are the allowed values for the Floquet modes. This defines two different classes $h_k^{e/o, l_{\max}}$ of finite-dimensional Floquet Hamiltonians with chiral symmetries $S_{e/o}$, respectively. In real space, we obtain two corresponding tight-binding Floquet Hamiltonians $h_{nn'}^{e/o, l_{\max}}$, where the integers n, n' label the unit cells of dimension $2d$ (including spin, band, and Floquet modes). The study of $h_{nn'}^{e/o, l_{\max}}$ turns out to be very useful since the TESs of interest with shortest localization length already appear

for small l_{\max} and convergence in l_{\max} is reached rapidly even for large $t_F \sim \Omega$.

Calculation of TESs— We now construct TESs via an exact numerical approach for a half-infinite gapped system, with unit cells labeled by $n = 1, 2, \dots$, described by the Hamiltonians $h_{nn'} \equiv \frac{\Omega}{2} + h_{nn'}^{e, l_{\max}}$ or $h_{nn'} \equiv h_{nn'}^{o, l_{\max}}$, in the even and odd case, respectively. The corresponding bulk Hamiltonian in k -space for the infinite system is denoted by h_k , which has a chiral symmetry $S \equiv S_{e,o}$ w.r.t. zero energy. To find zero-energy TESs, which decay exponentially for $n \rightarrow \infty$, we determine the zero energy bulk eigenstates of h_k with $\text{Im}(k) > 0$, such that their linear combination vanishes at unit cell $n = 0$ for all $2d$ bands. This procedure is applicable for all nearest-neighbor hopping models like the one given by Eq. (1) [50]. Since $D_k = \det(h_k)$ is a power series in $z = e^{-ik}$ containing z^{2d}, \dots, z^{-2d} , there are in total $4d$ roots of $D_k = 0$ in the complex plane of which $2d$ roots satisfy $\text{Im}(k) > 0$ since $D_{k^*} = D_k^*$ [which follows from $h_{k^*} = (h_k)^\dagger$]. Therefore, the number of allowed zero energy bulk solutions is the same as the number of boundary conditions and it is not a priori clear whether the solutions are linearly dependent for $n = 0$ to be able to fulfil the vanishing boundary condition. However, by exploiting chiral symmetry, we can write h_k in the chiral basis by using the projectors $P_{\pm} = \frac{1}{2}(1 \pm S)$ on the states with chirality \pm . Since $P_{\pm} h_k P_{\pm} = 0$, we find that h_k is nondiagonal in the chiral basis with the $d \times d$ -matrices $A_k^{\pm} = P_{\mp} h_k P_{\pm}$ defining the nondiagonal blocks. The TESs with chirality \pm follow then from the above scheme by finding the roots of $D_k^{\pm} = \det A_k^{\pm} = 0$ with $\text{Im}(k) > 0$. This reduces the number of boundary conditions to d and, since D_k^{\pm} contains the powers z^d, \dots, z^{-d} , the total number of roots is given by $2d$. Crucially, the $2d$ roots can be distributed in an arbitrary manner between the upper and lower half of the complex plane since $h_{k^*} = (h_k)^\dagger$ requires only $A_{k^*}^+ = (A_k^-)^\dagger$ and $D_{k^*}^+ = (D_k^-)^*$. Thus, if N_{\pm} is the number of roots of $D_k^{\pm} = 0$ with $\text{Im}(k) > 0$, the boundary condition can be satisfied by at least $Z_{\pm} = \max\{N_{\pm} - d, 0\}$ possibilities determining the number of TESs with chirality \pm (up to accidental cases not protected by chiral symmetry). We note that N_{\pm} is a topological invariant since this number can only change when at least one of the roots crosses the real axis which corresponds to a closing of the bulk gap. Using $D_{k^*}^+ = (D_k^-)^*$ we find that N_{\pm} is the number of roots of $D_k^+ = 0$ with $\text{Im}(k) \geq 0$. This gives $N_+ + N_- = 2d$ or $N_+ - d = -(N_- - d)$ and we conclude that *all* TESs must have the same chirality and the total number of TESs is given by

$$Z = \frac{1}{2} |N_+ - N_-|. \quad (2)$$

The details of our construction of TESs for chiral 1D systems is provided in the Supplemental Material (SM) containing also cases for special unit cells where the num-

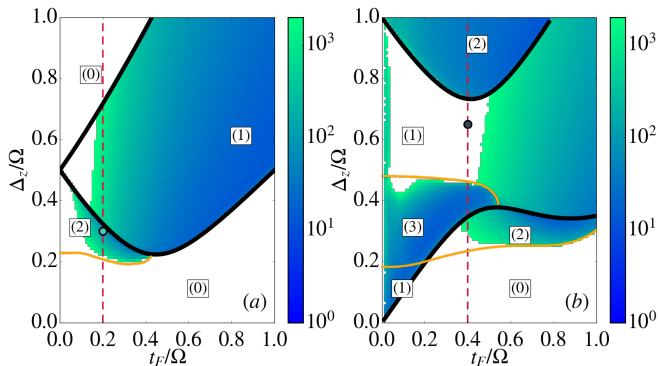


FIG. 1. Phase diagrams for (a) 2 and (b) 3 Floquet replicas. The black (orange) phase boundaries indicate transitions where the number of TEs is changing by an odd (even) number (so-called type “A” (“B”) phase transitions). In each phase region the number of TEs is indicated in the boxes. The color indicates the localization length ξ of the strongest-localized TES. The regions are colored in white if no TEs are present or if $\xi > 2000$. The vertical dashed lines indicate the values of t_F along which the position of the roots of $D_k^+ = 0$ are shown in Fig. 2 for 2 Floquet replicas (for 3 Floquet replicas see [47]). The dots indicate the parameter used in Fig. 3.

ber of boundary conditions can be further reduced [47].

In the SM, we also show that $\frac{1}{2}(N_+ - N_-)$ is identical to the winding number of $\det A_k^+$ [47], proving consistency with other approaches [52]. Furthermore, by applying our scheme to $h_k \equiv \frac{\Omega}{2} + h_k^{e,l_{\max}}$ and $h_k \equiv h_k^{o,l_{\max}}$, we can calculate the number $Z_{l_{\max}}^{e/o}$ of TEs at energy $E = -\frac{\Omega}{2}$ and $E = 0$ via Eq. (2). In the SM [47], we show without any truncation that $Z^{e/o} = \lim_{l_{\max} \rightarrow \infty} Z_{l_{\max}}^{e/o}$ are identical to the absolute values of the topological invariants ν_π/ν_0 defined in Ref. 5 via special time evolution operators. While proving consistent with earlier works, our approach via a truncated Floquet Hamiltonian in frequency space is essential to efficiently address the *most important* TEs, which are the ones with shortest localization length. Furthermore, we note that our scheme works as well for parabolic dispersion relations $E_k = k^2/(2m)$ or for linear Rashba terms $\alpha_k = \alpha k$ as they appear for continuum systems.

Phase diagram— Using the numerical approach described above we determine the TEs and the phase diagram as a function of t_F and Δ_Z . Corresponding to the two different gaps at $E = -\frac{\Omega}{2}, 0$ we show the phase diagrams for an even/odd truncation of the Floquet replicas, respectively, and consider different truncation orders to analyse convergence. For all figures we use the parameters $W = 8$, $\Omega = 0.4$, and $\alpha = 0.3$. First, we use a low (not yet converged) truncation order $l_{\max} = 1$. The number of TEs and the localization length [51] of the strongest-localized TES is shown in Fig. 1. To under-

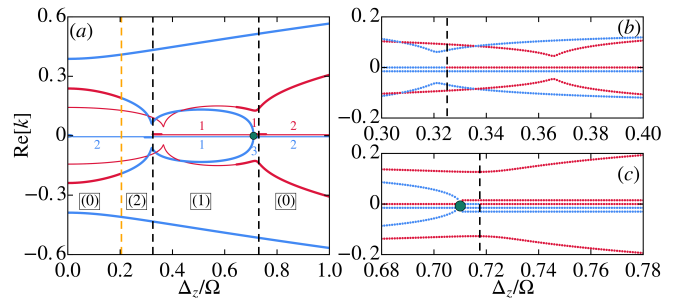


FIG. 2. Real parts $\text{Re}(k_i)$ of the roots of $D_{k_i}^+ = 0$ for 2 Floquet replicas as a function of Δ_Z at fixed $\frac{t_F}{\Omega} = 0.2$ (i.e., along the dashed line in Fig. 1(a)). Blue/red lines correspond to roots with $\text{Im}(k_i) \geq 0$. The vertical dashed lines correspond to phase transitions of type “A” (black) or “B” (orange). The two transitions of type “A” are shown on a smaller scale in (b) and (c). If the real part of several roots is zero we indicate their number in (a) and use a slight offset in (b) and (c). Thick lines in (a) indicate roots with $|\text{Im}(k_i)| < 0.14$, which dominate TEs (if present) and can be identified with the local minima in the bulk band structure (see Fig. 3(a) for $\frac{\Delta_Z}{\Omega} = 0.3$). The boxes in (a) contain the number of TEs in the various phases. The green dot in (a) and (c) indicates a bifurcation point which is very close to the phase transition.

stand the phase boundaries, we show in Fig. 2 the evolution of the real part $\text{Re}(k)$ of the roots of $D_k^+ = 0$ along the vertical dashed line in Fig. 1(a) (an analog figure is shown in the SM along the dashed line in Fig. 1(b) [47]), together with the sign of $\text{Im}(k)$ (indicated by blue/red color for \pm). There are two different classes of phase boundaries in Fig. 1 (in the following called “A” and “B”), where the number Z of TEs is either changing by an odd (black lines) or even (orange lines) number. A transition of type “A” occurs for a root crossing $k = 0$ along the imaginary axis which changes the number Z of TEs by one cf. Eq. (2). A transition of type “B” is associated with two roots crossing simultaneously the real axis at finite $\pm k_i$ [53] leading to a change of Z by two. At the phase transition, the bulk gap closes either at $k = 0$ (type “A”) or at finite $\pm k_i$ (type “B”). Therefore, phase boundaries of type “A” are independent of the SOI, whereas the ones of type “B” depend on α . Moreover, phase transitions of type “A” are often but not always associated with a bifurcation point lying quite close to the phase boundary (indicated by a green dot in Fig. 2(a,c)). A bifurcation point occurs when two roots with real parts $\pm k_i \neq 0$ merge on the imaginary axis and, subsequently, move along the imaginary axis in different directions such that one of the roots crosses through $k = 0$ at the phase transition. We note that, sufficiently apart from the phase boundaries and for sufficiently small values of t_F and Δ_Z , the real parts of the roots with small imaginary part (thick lines in Fig. 2) are related to the positions k_i of the local minima of the bulk band structure, see Fig. 3(a). Furthermore, the energy distance Δ_i

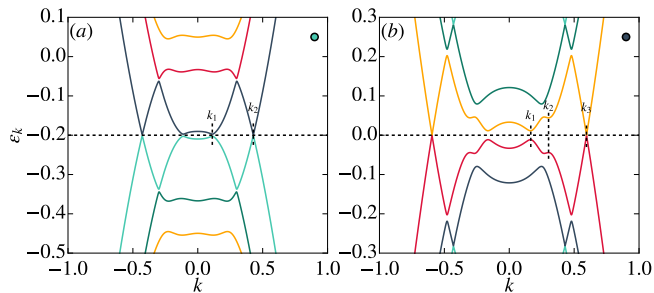


FIG. 3. Band structure for (a) 2 and (b) 3 Floquet replicas with (a) $(\frac{t_F}{\Omega}, \frac{\Delta_Z}{\Omega}) = (0.2, 0.3)$ and (b) $(\frac{t_F}{\Omega}, \frac{\Delta_Z}{\Omega}) = (0.4, 0.65)$ (corresponding to the parameter values at the dots in Fig. 1). The label k_i denote the positions of the local band minima which can be related to the real parts of the roots with small imaginary part in Fig. 2 (and a corresponding figure in the SM for 3 Floquet replicas [47]). The gaps at (a) $\pm k_{1,2}$ and (b) $\pm k_3$ are too small to be visible on the chosen scale.

of the bulk energy ϵ_{k_i} from the gap center agrees roughly (up to a factor of $O(1)$) with the imaginary part κ_i of the roots via $\kappa_i \sim \frac{\Delta_i}{v_i}$, with $v_i = (\partial_k E)_{k_i} = \frac{W}{2} \sin(k_i)$. However, for larger values of t_F and Δ_Z as indicated in Fig. 3(b), the Floquet bands are strongly coupled leading to a significant broadening of the anticrossings and minima at small k , and there is no possibility to set up effective theories treating each anticrossing separately and coupling them perturbatively.

Of particular interest are the phase diagram regions where the strongest-localized TES has a small localization length (blue regions in Fig. 1) and is formed from roots with small real part (where the imaginary part is larger, see also the band structure shown in Fig. 3(b)). In this case the strongest-localized TES can coexist with other TESs of larger localization length since they have all the same chirality (also called “sublattice”) and can not repel each other. This important feature persists for higher truncation order.

The phase diagram for a truncation with 6 and 5 Floquet replicas is shown in Fig. 4. We have presented only those phase boundaries which do not change significantly by increasing the truncation order. This does not exclude that further pairs of TESs can arise from very small gaps at large k not captured in the considered truncation order leading to additional phase boundaries. However, these TESs have a very large localization length far beyond those ones occurring in Fig. 4 and are of minor interest. Therefore, the most important feature in the phase diagram is *not* the total number of TESs (which converges slowly) but the identification of those regions where the strongest-localized TES has a small localization length (which converges always very fast). Besides the RWA phase [indicated by a red-dashed contour in Fig. 4(b)], there are many new regions in the phase diagram with TESs of comparable localization length to the one occur-

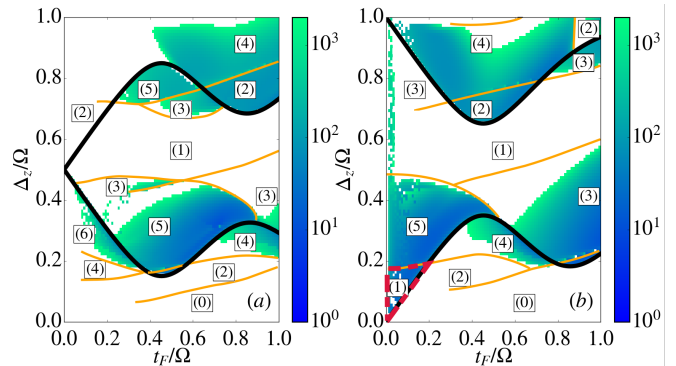


FIG. 4. Phase diagrams for (a) 6 and (b) 5 Floquet replicas (same notations as in Fig. 1). All phase boundaries shown are almost converged and do not change significantly by increasing the truncation order (some of them end at small t_F due to numerical instabilities). The red-dashed contour in (b) indicates the RWA phase where $t_F, \Delta_Z \ll \Omega$.

ring in the RWA phase. Furthermore, we find that the RWA phase is extended to the surprisingly large region $t_F < \Delta_Z \lesssim \frac{\Omega}{2}$ but for $0.2 \lesssim \Delta_Z \lesssim \frac{\Omega}{2}$ additional TESs are present besides the strongly localized RWA state. The strongly localized TESs occurring already at a low truncation order are stable, since a closing of very small gaps at anticrossings with large k will give the TESs only a very small broadening but will not influence their localization length significantly.

We have complemented our results by an exact diagonalization study on a finite system with $N = 10000$ unit cells showing consistency as well as the occurrence of finite energy nontopological edge states

Conclusions— We have analyzed the topological properties of chiral 1D FTIs beyond RWA and have developed a method to deal with the occurrence of many anticrossings of Floquet replicas. This unique feature of FTIs is shown to lead to many new regions in the topological phase diagram with TESs of very short localization length accessible to experiments. Regions with multiple TESs with the same chirality could be useful as realizations of qudits (which are d -dimensional extensions of qubits). We analyzed driven Rashba nanowires as a concrete Floquet model, which we propose can be put to an experimental test in curved bilayer graphene, where both the models parameters, band gap and the Rashba term, can be tuned by external parameters [48]. The presence of TESs can be detected most accurately via STM transport spectroscopy which probes resonances of the spectral density inside the gap and is not sensitive to the rather subtle occupation of the Floquet states. Moreover, our proposed approach via a truncated Floquet Hamiltonian may also be useful for a further development of other methods analysing topological states like, e.g., the scattering state formalism [8].

We thank V. Meden and S. Wessel for fruitful dis-

cussions. This work was supported by the Deutsche Forschungsgemeinschaft via RTG 1995, the Swiss National Science Foundation (SNSF) and NCCR QSIT. Simulations were performed with computing resources granted by RWTH Aachen University under projects rwth0347, rwth0362, thes0445, and prep0010. Funding was received from the European Union's Horizon 2020 research, innovation program (ERC Starting Grant, grant agreement No 757725) as well as from the independence grant from the TR 183 network.

* Email: schoeller@physik.rwth-aachen.de

- [1] T. Kitagawa, E. Berg, M. Rudner, and E. Demler, Phys. Rev. B **82**, 235114 (2010).
- [2] T. Kitagawa, M.S. Rudner, E. Berg, and E. Demler, Phys. Rev. A **82**, 033429 (2010).
- [3] M.S. Rudner, N.H. Lindner, E. Berg, and M. Levin, Phys. Rev. X **3**, 031005 (2013).
- [4] J.K. Asbóth and H. Obuse, Phys. Rev. B **88**, 121406(R) (2013).
- [5] J.K. Asbóth, B. Tarasinski, and P. Delplace, Phys. Rev. B **90**, 125143 (2014).
- [6] F. Nathan and M. S. Rudner, New J. Phys. **17**, 125014 (2015).
- [7] D. Carpentier, P. Delplace, M. Fruchart, and K. Gawedzki, Phys. Rev. Lett. **114**, 106806 (2015).
- [8] I.C. Fulga and M. Maksymenko, Phys. Rev. B **93**, 075405 (2016).
- [9] M. Fruchart, Phys. Rev. B **93**, 115429 (2016).
- [10] R. Roy and F. Harper, Phys. Rev. B **95**, 195128 (2017); *ibid.* **96**, 155118 (2017).
- [11] S. Yao, Z. Yan and Z. Wang, Phys. Rev. B **96**, 195303 (2017).
- [12] B. Höckendorf, A. Alvermann, and H. Fehske, Phys. Rev. B **97**, 045140 (2018).
- [13] T. Kitagawa, M.A. Broome, A. Fedrizzi, M.S. Rudner, E. Berg, I. Kassal, A. Aspuru-Guzik, E. Demler, and A.G. White, Nat. Commun. **3**, **882** (2012).
- [14] M.C. Rechtsman, J.M. Zeuner, Y. Plotnik, Y. Lumer, D. Podolsky, F. Dreisow, S. Nolte, M. Segev, and A. Szameit, Nature (London) **496**, 196 (2013).
- [15] L. Lu, J.D. Joannopoulos, and M. Soljacic, Nat. Photon. **8**, 821 (2014).
- [16] F. Cardano, A. D'Errico, A. Dauphin, M. Maffei, B. Piccirillo, C. de Lisio, G. De Filippis, V. Cataudella, E. Santamato, L. Marrucci, M. Lewenstein, and P. Massignan, Nat. Commun. **8**, 15516 (2017).
- [17] L.J. Maczewsky, J.M. Zeuner, S. Nolte, and A. Szameit, Nat. Commun. **8**, 13756 (2017).
- [18] S. Mukherjee, A. Spracklen, M. Valiente, E. Andersson, P. Öhberg, N. Goldman, and R.R. Thomson, Nat. Comm. **8**, 13918 (2017).
- [19] G. Jotzu, M. Messer, R. Desbuquois, M. Lebrat, T. Uehlinger, D. Greif, and T. Esslinger, Nature (London) **515**, 237 (2014).
- [20] K. Jiménez-García, L.J. LeBlanc, R.A. Williams, M.C. Beeler, C. Qu, M. Gong, C. Zhang, and I.B. Spielman, Phys. Rev. Lett. **114**, 125301 (2015).
- [21] A. Quelle, C. Weitenberg, K. Sengstock, and C. Morais Smith, New J. Phys. **19**, 113010 (2017).
- [22] H.L. Calvo, H.M. Pastawski, S. Roche, and L.E.F. Foa Torres, Appl. Phys. Lett. **98**, 232103 (2011).
- [23] E. Suárez Morell and L.E.F. Foa Torres, Phys. Rev. B **86**, 125449 (2012).
- [24] Y.H. Wang, H. Steinberg, P. Jarillo-Herrero, and N. Gedik, Science **342**, 453 (2013).
- [25] G. Usaj, P.M. Perez-Piskunow, L.E.F. Foa Torres, and C.A. Balseiro, Phys. Rev. B **90**, 115423 (2014).
- [26] E.J. Sie, J.W. McIver, Yi-Hsien Lee, L. Fu, J. Kong, and N. Gedik, Nature Materials **14**, 290 (2015).
- [27] H.L. Calvo, L.E.F. Foa Torres, P.M. Perez-Piskunow, C.A. Balseiro, and G. Usaj, Phys. Rev. B **91**, 241404 (2015).
- [28] Y. Wang, Y. Liu, and B. Wang, Sci. Rep. **7**, 41644 (2017).
- [29] L. Jiang, T. Kitagawa, J. Alicea, A.R. Akhmerov, D. Pekker, G. Refael, J.I. Cirac, E. Demler, M.D. Lukin, and P. Zoller, Phys. Rev. Lett. **106**, 220402 (2011).
- [30] A. Kundu and B. Seradjeh, Phys. Rev. Lett. **111**, 136402 (2013).
- [31] A.A. Reynoso and D. Frustaglia, Phys. Rev. B **87**, 115420 (2013).
- [32] M. Thakurathi, A.A. Patel, D. Sen, and A. Dutta, Phys. Rev. B **88**, 155133 (2013).
- [33] M. Thakurathi, K. Sengupta, and D. Sen, Phys. Rev. B **89**, 235434 (2014).
- [34] M. Thakurathi, D. Loss, and J. Klinovaja, Phys. Rev. B **95**, 155407 (2017).
- [35] T. Oka and H. Aoki, Phys. Rev. B **79**, 081406 (2009).
- [36] J.-I. Inoue and A. Tanaka, Phys. Rev. Lett. **105**, 017401 (2010).
- [37] N.H. Lindner, G. Refael, and V. Galitski, Nat. Phys. **7**, 490 (2011).
- [38] B. Dóra, J. Cayssol, F. Simon, and R. Moessner, Phys. Rev. Lett. **108**, 056602 (2012).
- [39] P.M. Perez-Piskunow, L.E.F. Foa Torres, and G. Usaj, Phys. Rev. A **91**, 043625 (2015); in this reference also the case $t_F, \omega \gtrsim 0.1W$ has been studied which is orthogonal to our parameter regime.
- [40] N.H. Lindner, D.L. Bergman, G. Refael, and V. Galitski, Phys. Rev. B **87**, 235131 (2013).
- [41] J. Klinovaja, P. Stano, and D. Loss, Phys. Rev. Lett. **116**, 176401 (2016).
- [42] We set \hbar and the lattice spacing to unity throughout this work.
- [43] A. Gómez-León and G. Platero, Phys. Rev. Lett. **110**, 200403 (2013).
- [44] M. Rodríguez-Vega and B. Seradjeh, Phys. Rev. Lett. **121**, 036402 (2018).
- [45] M. Rodríguez-Vega, M. Lentz, and B. Seradjeh, New J. Phys. **20**, 093022 (2018).
- [46] Our method can be applied to the class *CII* and *AIII* as well and further generalizations will be described in a future work, see also [47].
- [47] See Supplemental Material.
- [48] J. Klinovaja, G.J. Ferreira, and D. Loss, Phys. Rev. B **86**, 235416 (2012).
- [49] Y. Oreg, G. Refael, and F. von Oppen, Phys. Rev. Lett. **105**, 177002 (2010).
- [50] This can always be achieved by taking the unit cell large enough.
- [51] The localization length ξ of the TESs is calculated from the inverse participation ratio (IPR).
- [52] S. Ryu, A.P. Schnyder, A. Furusaki, and A.W.W. Lud-

wig, New J. Phys. **12**, 065010 (2010).

[53] Due to time-reversal symmetry of the model Eq. (1), the

roots with finite real part appear in pairs at k_i and $-k_i^*$.

Chiral 1D Floquet topological insulators beyond rotating wave approximation Supplemental Material

Dante M. Kennes,¹ Niclas Müller,² Mikhail Pletyukhov,² Clara Weber,² Christoph Bruder,³ Fabian Hassler,⁴ Jelena Klinovaja,³ Daniel Loss,³ and Herbert Schoeller^{2,*}

¹*Dahlem Center for Complex Quantum Systems and Fachbereich Physik,
Freie Universität Berlin, 14195 Berlin, Germany*

²*Institut für Theorie der Statistischen Physik, RWTH Aachen, 52056 Aachen,
Germany and JARA - Fundamentals of Future Information Technology*

³*Department of Physics, University of Basel, Klingelbergstrasse 82, CH-4056 Basel, Switzerland*

⁴*JARA-Institute Quantum Information, RWTH Aachen University, 52056 Aachen, Germany*

(Dated: May 14, 2020)

The following appendices comprise the Supplemental Material to Ref. 1: (1) We will present the proof of the bulk-boundary correspondence and the construction of the topological edge states (TESSs) in the general case together with the relation to the concept of topological invariants defined via winding numbers for the static as well as for the dynamic (Floquet) case. (2) We relate the phase diagram for 3 Floquet replicas to the evolution of the roots of the determinant of the nondiagonal blocks of the Hamiltonian in the chiral basis. (3) We present the results from the exact diagonalization study for a finite system and discuss the occurrence of nontopological edge states.

I. BULK-BOUNDARY CORRESPONDENCE AND CONSTRUCTION OF TESS

A generic tight-binding model for a half-infinite chain with an even number of bands (required for chiral symmetry) can be written as

$$H = \sum_{n=1}^{\infty} \{ |n\rangle\langle n| \otimes h(0) + |n+1\rangle\langle n| \otimes h(1) + |n\rangle\langle n+1| \otimes h(-1) \}, \quad (1)$$

where $n = 1, 2, \dots$ labels the unit cells with $2d$ bands and $h(\delta) = h(-\delta)^\dagger$, $\delta = 0, \pm 1$, are $2d \times 2d$ -matrices describing the hopping processes from unit cell n to $n + \delta$. We have taken the unit cell large enough such that only nearest-neighbor hopping processes occur. Assuming a local chiral symmetry $S = S^\dagger = S^{-1}$ such that

$$Sh(\delta)S = -h(\delta) \quad , \text{ for } \delta = 0, \pm 1, \quad (2)$$

we can decompose $h(\delta)$ as

$$h(\delta) = A^+(\delta) + A^-(\delta) \quad , \quad A^+(\delta) = P_- h(\delta) P_+ \quad , \quad A^-(\delta) = P_+ h(\delta) P_- = A^+(-\delta)^\dagger, \quad (3)$$

where $P_\pm = \frac{1}{2}(1 \pm S)$ project on the subspaces with chirality \pm . In the same way we can split the total Hamiltonian of the half-infinite chain as

$$H = A^+ + A^- \quad , \quad A^+ = P_- H P_+ \quad , \quad A^- = P_+ H P_- = (A^+)^\dagger, \quad (4)$$

with

$$A^\pm = \sum_{n=1}^{\infty} \{ |n\rangle\langle n| \otimes A^\pm(0) + |n+1\rangle\langle n| \otimes A^\pm(1) + |n\rangle\langle n+1| \otimes A^\pm(-1) \}. \quad (5)$$

In addition we define the corresponding quantities for the bulk where we sum over all unit cells

$$H_{\text{bulk}} = \sum_{n=-\infty}^{\infty} \{ |n\rangle\langle n| \otimes h(0) + |n+1\rangle\langle n| \otimes h(1) + |n\rangle\langle n+1| \otimes h(-1) \}, \quad (6)$$

$$A_{\text{bulk}}^\pm = \sum_{n=-\infty}^{\infty} \{ |n\rangle\langle n| \otimes A^\pm(0) + |n+1\rangle\langle n| \otimes A^\pm(1) + |n\rangle\langle n+1| \otimes A^\pm(-1) \}, \quad (7)$$

which can be written in quasimomentum space $|k\rangle = \frac{1}{\sqrt{2\pi}} \sum_{n=-\infty}^{\infty} e^{ikn} |n\rangle$, $-\pi < k \leq \pi$, in the diagonal form

$$H_{\text{bulk}} = \int_{-\pi}^{\pi} dk |k\rangle\langle k| \otimes h_k \quad , \quad A_{\text{bulk}}^{\pm} = \int_{-\pi}^{\pi} dk |k\rangle\langle k| \otimes A_k^{\pm} \quad , \quad (8)$$

with

$$h_k = \sum_{\delta=0,\pm 1} e^{-ik\delta} h(\delta) = (h_k)^{\dagger} = A_k^+ + A_k^- \quad , \quad A_k^{\pm} = \sum_{\delta=0,\pm 1} e^{-ik\delta} A^{\pm}(\delta) = (A_k^{\mp})^{\dagger} \quad . \quad (9)$$

The goal is to find a TES $|\psi^{\pm}\rangle$ with zero energy $H|\psi^{\pm}\rangle = 0$ and chirality $S|\psi^{\pm}\rangle = \pm|\psi^{\pm}\rangle$ exponentially decaying for $n \rightarrow \infty$. Using (4) this means that we have to solve the equations

$$A^+|\psi^+\rangle = 0 \quad , \quad A^-|\psi^-\rangle = 0 \quad . \quad (10)$$

To construct the TES we make the following ansatz in unit cell n

$$|\psi^{\pm}(n)\rangle = \sum_{i=1}^{N_{\pm}} \lambda_i^{\pm} |\psi_{k_i}^{\pm}(n)\rangle \quad , \quad (11)$$

where $|\psi_{k_i}^{\pm}\rangle$ are solutions of the bulk problem with complex quasimomentum k_i in the upper half of the complex plane $\text{Im}k_i > 0$, and zero energy

$$|\psi_{k_i}^{\pm}(n)\rangle = |\chi_{k_i}^{\pm}\rangle e^{ik_i n} \quad , \quad A_{k_i}^{\pm} |\chi_{k_i}^{\pm}\rangle = 0 \quad . \quad (12)$$

Inserting the ansatz (11) in (10) we get with (5) for unit cell $n \geq 1$

$$\begin{aligned} \langle n|A^{\pm}|\psi^{\pm}\rangle &= \sum_{m=1}^{\infty} \sum_{\delta=0,\pm 1} \langle n|m+\delta\rangle A^{\pm}(\delta) |\psi^{\pm}(m)\rangle \\ &= \delta_{n1} \sum_{\delta=0,-1} A^{\pm}(\delta) |\psi^{\pm}(1-\delta)\rangle + \delta_{n>1} \sum_{\delta=0,\pm} A^{\pm}(\delta) |\psi^{\pm}(n-\delta)\rangle \\ &= -\delta_{n1} A^{\pm}(1) |\psi^{\pm}(0)\rangle + \sum_{\delta=0,\pm} A^{\pm}(\delta) |\psi^{\pm}(n-\delta)\rangle \\ &= -\delta_{n1} A^{\pm}(1) |\psi^{\pm}(0)\rangle + \sum_{i=1}^{N_{\pm}} \lambda_i^{\pm} e^{ik_i n} \sum_{\delta=0,\pm} A^{\pm}(\delta) e^{-ik_i \delta} |\chi_{k_i}^{\pm}\rangle \\ &= -\delta_{n1} A^{\pm}(1) |\psi^{\pm}(0)\rangle + \sum_{i=1}^{N_{\pm}} \lambda_i^{\pm} e^{ik_i n} A_{k_i}^{\pm} |\chi_{k_i}^{\pm}\rangle \\ &= -\delta_{n1} A^{\pm}(1) |\psi^{\pm}(0)\rangle \quad , \end{aligned} \quad (13)$$

where we have used (11), (12), and (9) in the last three steps. Thus, we have to fulfil the following boundary condition on an artificial unit cell at $n = 0$

$$A^{\pm}(1) |\psi^{\pm}(0)\rangle = A^{\pm}(1) \sum_{i=1}^{N_{\pm}} \lambda_i^{\pm} |\chi_{k_i}^{\pm}\rangle = 0 \quad . \quad (14)$$

This boundary condition is obviously fulfilled for $\sum_{i=1}^{N_{\pm}} \lambda_i^{\pm} |\chi_{k_i}^{\pm}\rangle = 0$ but the number of boundary conditions can be reduced if the $d \times d$ -matrices $A^+(1)$ and $A^-(1) = A^+(-1)^{\dagger}$ contain zero matrix elements, which are connected to some symmetries assumed for the model under consideration. If by permuting rows and columns, one can find r_{\pm} rows and s_{\pm} columns of $A^+(\pm 1)$ which are zero (possibly after some common unitary transformation which commutes with the chiral symmetry), then the number of boundary conditions is given by $d_{\pm} = \min\{r_{\pm}, s_{\pm}\}$. These numbers are directly related to the powers of $\det A_k^{\pm}$ in $z = e^{-ik}$, since $A_k^+ = A^+(0) + e^{-ik} A^+(1) + e^{ik} A^+(-1)$, which gives

$$\det A_k^+ \rightarrow z^{d_+} , z^{d_+-1} , \dots , z^{-d_-+1} , z^{-d_-} \quad . \quad (15)$$

The total number of solutions of (12) is given by the number N_{\pm} of solutions of $\det A_k^{\pm} = 0$ for k in the upper half of the complex plane, i.e. $\text{Im}(k) > 0$ and $-\pi < \text{Re}(k) \leq \pi$. Since d_{\pm} boundary conditions have to be fulfilled this means that it is guaranteed that at least

$$Z_{\pm} = \max\{N_{\pm} - d_{\pm}, 0\} \quad (16)$$

solutions can be found for the set of coefficients $\{\lambda_i^{\pm}\}_i$ in (11), up to additional accidental solutions which are not protected by symmetry. Z_{\pm} is the number of TESs with chirality \pm . Since $A_k^- = (A_{k^*}^+)^{\dagger}$ for complex k (see Eq. (9) for real k) we get $\det A_k^- = (\det A_{k^*}^+)^*$, i.e. the number of solutions of $\det A_k^- = 0$ in the upper half of the complex plane is identical to the number of solutions of $\det A_{k^*}^+ = 0$ in the lower half of the complex plane. We conclude that N_{\pm} is the number of solutions of $\det A_k^{\pm} = 0$ for $\text{Im}(k) \gtrless 0$. Using (15), the total number $N_+ + N_-$ of solutions of $\det A_k^{\pm} = 0$ in the complex plane with $-\pi < \text{Re}(k) \leq \pi$ is given by $d_+ + d_-$, which gives the important equation

$$N_+ - d_+ = -(N_- - d_-). \quad (17)$$

Together with (16) we find the final result for the total number Z of TESs

$$Z = Z_+ + Z_- = \frac{1}{2}|N_+ - N_- - (d_+ - d_-)|. \quad (18)$$

We note that the construction of the TESs via (11) and (12) does not work if several solutions of $\det A_k^{\pm} = 0$ coincide (i.e. the case of multiple roots). At such special bifurcation points the ansatz for the TES has to be an exponential together with a pre-exponential polynomial. However, these are very special points in the phase diagram with mass zero and the formula (18) for the number Z of TESs is not changed if one includes in N_{\pm} the multiplicity of each root.

Our approach can as well be used for the chiral classes *CII* and *AIII* in *1D*. In class *CII* Kramers pairs will occur for all TESs due to time-reversal symmetry with $T^2 = -1$. In class *AIII* neither time-reversal nor particle-hole symmetry is fulfilled. This has the only consequence that the solutions of Eq. (12) do no longer occur in time-reversed pairs k_i and $-k_i^*$, with the effect that a topological phase transition changing the parity of the number of TESs can also happen at finite k .

In case chiral symmetry is not fulfilled or if the number of roots of $\det A_k^{\pm} = 0$ with $\text{Im}(k_i) \gtrless 0$ is the same (as can be shown for the chiral classes *DIII* and *CI*), it is also possible to study the TESs by calculating all $N = 2d$ solutions of

$$h_{k_i} |\chi_{k_i}\rangle = 0 \quad , \quad \text{Im}(k_i) > 0, \quad (19)$$

and constructing the wave function of the TES by

$$|\psi(n)\rangle = \sum_{i=1}^N \lambda_i |\psi_{k_i}\rangle \quad , \quad |\psi_{k_i}\rangle = |\chi_{k_i}\rangle e^{ik_i n}, \quad (20)$$

provided that the boundary condition $\sum_{i=1}^N \lambda_i |\chi_{k_i}\rangle = 0$ can be fulfilled. Although the number N of solutions is identical to the dimension of the vectors χ_{k_i} , this can be easily checked numerically by analysing the rank r of the matrix of all eigenvectors χ_{k_i} . If $r < 2d$ the eigenvectors are linearly dependent and the boundary condition can be fulfilled.

Furthermore, we note that also the topological classes *D* and *DIII* in *1D* with \mathbb{Z}_2 -symmetry can be studied by a variant of our proposed method for chiral systems and higher dimensions can be analysed by dimensional reduction. This goes beyond the scope of the present work and requires a systematic study and classification of all topological systems which will be part of future works².

Our proposed method to calculate the TESs via the bulk properties of the system relies essentially on translational invariance along the periodic lattice. In the presence of disorder translational invariance is broken and our method can not be applied. However, the stability of a certain TES can still be studied by comparing the disorder-induced broadening Γ with the corresponding gap Δ of the dispersion relation in which the TES is sitting. If $\Gamma \ll \Delta$, the TES is coupled only weakly to the bulk spectrum and its stability will be preserved. For weak disorder, a rough estimation of Γ can be obtained via golden rule in perturbation theory. This requires also the knowledge of all bulk states in the absence of disorder. These states can also be calculated by our method. A bulk solution is again of the form (20) but in addition there are two solutions of (19) with $\text{Im}(k_i) = 0$, besides $2d - 1$ solutions with $\text{Im}(k_i) > 0$ and $2d - 1$ solutions with $\text{Im}(k_i) < 0$ (giving $4d$ solutions in total). This means that there are in total $2d + 1$ solutions with $\text{Im}(k_i) \geq 0$ which is sufficient to fulfil $2d$ boundary conditions.

II. WINDING NUMBERS FOR CHIRAL STATIC HAMILTONIANS

The number Z of TEs given by Eq. (18) via the number N_{\pm} of roots of the function $f_k = \det A_k^+$ in the upper/lower half of the complex plane for $-\pi < \text{Re}(k) \leq \pi$ can be related to its winding number ν around the origin when k changes on the real axis from $-\pi \rightarrow \pi$

$$\nu = \frac{1}{2\pi i} \int_{-\pi}^{\pi} dk \frac{f'_k}{f_k}, \quad (21)$$

where $f'_k = \frac{df_k}{dk}$ is the derivative and the winding is defined positive for counterclockwise rotation here. In the following we will show that

$$\nu = N_+ - d_+ = -(N_- - d_-) \quad \Rightarrow \quad |\nu| = Z, \quad (22)$$

where we have used (17) and (18) for the second and third identity. Therefore it is sufficient to prove that $\nu = N_+ - d_+$.

To find this relation we use the argument principle which gives the following relation for the number of roots of an analytic function f_k inside any closed contour γ in the complex plane

$$N_{\gamma} = \frac{1}{2\pi i} \oint_{\gamma} dk \frac{f'_k}{f_k}, \quad (23)$$

where the direction of γ is counterclockwise. Choosing for γ a closed curve consisting of four straight lines according to $-\pi \rightarrow \pi \rightarrow \pi + i\infty \rightarrow -\pi + i\infty \rightarrow -\pi$, we surround obviously all roots of f_k in the upper half, i.e. $N_{\gamma} = N_+$. Using (21) the path from $-\pi \rightarrow \pi$ gives the winding number ν . Since f_k is periodic in $k \rightarrow k + 2\pi$, the two contributions from $\pi \rightarrow \pi + i\infty$ and $-\pi + i\infty \rightarrow -\pi$ cancel each other. Thus, we get

$$N_+ = \nu - \frac{1}{2\pi i} \int_{-\pi + i\infty}^{\pi + i\infty} dk \frac{f'_k}{f_k}. \quad (24)$$

For $\text{Im}(k) \rightarrow \infty$ we find from (15) that $f_k = ae^{-ikd_+}$ with some k -independent prefactor a . This leads to $\frac{f'_k}{f_k} = -id_+$ and the second term on the r.h.s. of (24) gives d_+ . This gives the desired relation $\nu = N_+ - d_+$.

The winding number can be expressed in many alternative ways. Using $\frac{f'_k}{f_k} = \frac{d}{dk} \ln(\det A_k^+) = \frac{d}{dk} \text{Tr} \ln(A_k^+)$ we can write

$$\nu = \frac{1}{2\pi i} \int_{-\pi}^{\pi} \text{Tr}(A_k^+)^{-1} dA_k^+. \quad (25)$$

Instead of A_k^+ one can also use the unitary q -matrix $q_k = \frac{1}{\sqrt{A_k^+(A_k^+)^{\dagger}}} A_k^+$. Since the winding number of a hermitian matrix is zero we get

$$\nu = \frac{1}{2\pi i} \int_{-\pi}^{\pi} \text{Tr} q_k^{\dagger} dq_k. \quad (26)$$

The q -matrix can be expressed in a compact way via the representation of the Hamiltonian in a basis of eigenstates $|x_{k\sigma}^{\alpha}\rangle$ ($\alpha = 1, \dots, d$; $\sigma = \pm$) such that

$$h_k |x_{k\sigma}^{\alpha}\rangle = \sigma \epsilon_k^{\alpha} |x_{k\sigma}^{\alpha}\rangle, \quad S |x_{k\sigma}^{\alpha}\rangle = |x_{k\bar{\sigma}}^{\alpha}\rangle, \quad (27)$$

with $\bar{\sigma} = -\sigma$ and $\epsilon_k^{\alpha} > 0$. This is always possible for a gapped Hamiltonian with chiral symmetry. In this basis the projectors $P_{\pm} = \frac{1}{2}(1 \pm S)$ act as follows

$$P_+ |x_{k\sigma}^{\alpha}\rangle = P_+ |x_{k+}^{\alpha}\rangle, \quad P_- |x_{k\sigma}^{\alpha}\rangle = \sigma P_- |x_{k+}^{\alpha}\rangle. \quad (28)$$

This gives for the matrix $A_k^+ = P_- h_k P_+$ the result

$$A_k^+ = \sum_{\alpha\sigma} \sigma \epsilon_k^{\alpha} P_- |x_{k\sigma}^{\alpha}\rangle \langle x_{k\sigma}^{\alpha}| P_+ \quad (29)$$

$$= 2 \sum_{\alpha} \epsilon_k^{\alpha} P_- |x_{k+}^{\alpha}\rangle \langle x_{k+}^{\alpha}| P_+, \quad (30)$$

and the following result for the q -matrix

$$q_k = 2 \sum_{\alpha} P_- |x_{k+}^{\alpha}\rangle \langle x_{k+}^{\alpha}| P_+. \quad (31)$$

Using $2\langle x_{k+}^{\alpha}|P_{\sigma}|x_{k+}^{\alpha'}\rangle = \delta_{\alpha\alpha'}$ we find after some straightforward algebra the following useful result for the integrand of the winding number (26)

$$\text{Tr } q_k^{\dagger} dq_k = 2 \sum_{\alpha} \langle x_{k+}^{\alpha}|S|dx_{k+}^{\alpha}\rangle = 2 \sum_{\alpha} \langle x_{k-}^{\alpha}|S|dx_{k-}^{\alpha}\rangle, \quad (32)$$

where we used $S^2 = 1$ and $S|x_{k+}^{\alpha}\rangle = |x_{k-}^{\alpha}\rangle$ in the last step.

III. WINDING NUMBERS FOR CHIRAL FLOQUET HAMILTONIANS

We start from a time-dependent periodic Hamiltonian $h_k(t) = h_k(t+T) = h_k(t)^{\dagger}$ with oscillation frequency $\Omega = \frac{2\pi}{T}$ in quasimomentum representation which has the local chiral symmetry

$$Sh_k(t)S = -h_k(-t). \quad (33)$$

The corresponding Floquet-Hamiltonian h_k^F is defined by

$$(h_k^F)_{ll'} = h_{k,l-l'} - l\Omega\delta_{ll'}, \quad (34)$$

where

$$|l\rangle = \int_0^T dt |t\rangle \langle t|l\rangle, \quad \langle t|l\rangle = \frac{1}{\sqrt{T}} e^{-i\Omega t} \quad (35)$$

denote the Floquet modes and

$$h_{k,l} = \frac{1}{T} \int_0^T dt e^{i\Omega t} h_k(t) = h_{k,-l}^{\dagger} \quad (36)$$

are the discrete Fourier components of $h_k(t)$ which fulfil the chiral symmetry

$$Sh_{k,l}S = -h_{k,-l}. \quad (37)$$

Due to the Bloch theorem all solutions of the time-dependent Schrödinger equation of $h_k(t)$ can be determined from the eigenvectors $|x_k\rangle$ of the Floquet Hamiltonian h_k^F with quasienergy ϵ_k as

$$\psi_k(t) = \sqrt{T} e^{-i\epsilon_k t} |x_k(t)\rangle, \quad (38)$$

where

$$|x_k(t)\rangle = \langle t|x_k\rangle = \sum_l \langle t|l\rangle \langle l|x_k\rangle = \frac{1}{\sqrt{T}} \sum_l e^{-i\Omega t} |x_{k,l}\rangle \quad (39)$$

is the Fourier transform of $|x_{k,l}\rangle = \langle l|x_k\rangle$ w.r.t. to the Floquet modes. The quasienergy is defined uniquely up to multiples of Ω since the Floquet Hamiltonian transforms in the following way under translations $T_r|l\rangle = |l+r\rangle$ of the Floquet modes

$$T_r h_k^F T_{-r} = h_k^F + r\Omega. \quad (40)$$

This means that

$$h_k^F |x_k\rangle = \epsilon_k |x_k\rangle \quad \Rightarrow \quad h_k^F T_{-r} |x_k\rangle = (\epsilon_k + r\Omega) T_{-r} |x_k\rangle. \quad (41)$$

Due to (34), (37) and (40) we find that h_k^F has two independent chiral symmetries S_F and \bar{S}_F w.r.t. the two energies $E = 0$ and $E = -\frac{\Omega}{2}$ (both modulo Ω) defined by

$$S_F = PS, \quad \bar{S}_F = T_1 PS, \quad (42)$$

where $P|l\rangle = |-l\rangle$ changes the parity of the Floquet modes. This means that with $\bar{h}_k^F = h_k^F + \frac{\Omega}{2}$ we get

$$S_F h_k^F S_F = -h_k^F \quad , \quad \bar{S}_F \bar{h}_k^F \bar{S}_F = -\bar{h}_k^F . \quad (43)$$

We note that the chiral symmetry remains even if the Floquet Hamiltonian h_k^F (\bar{h}_k^F) is truncated with an odd (even) number of Floquet modes $l = -l_{\max}, \dots, l_{\max}$ ($l = -l_{\max} + 1, \dots, l_{\max}$). According to (26) this allows the definition of two winding numbers via two q -matrices q_k^F and \bar{q}_k^F corresponding to S_F and \bar{S}_F , respectively

$$\nu = \frac{1}{2\pi i} \int_{-\pi}^{\pi} \text{Tr}(q_k^F)^\dagger dq_k^F \quad , \quad \bar{\nu} = \frac{1}{2\pi i} \int_{-\pi}^{\pi} \text{Tr}(\bar{q}_k^F)^\dagger d\bar{q}_k^F . \quad (44)$$

Due to (22) these topological invariants correspond to the number of TESs at energies $E = 0$ and $E = -\frac{\Omega}{2}$ even for a truncated Floquet Hamiltonian. For finite truncation it is impossible to relate the invariants to other invariants defined in the literature via the time evolution operators $U_k(T, 0)$ and $U_k(\frac{T}{2}, -\frac{T}{2})$ of $h_k(t)$, where no truncation is used³. Therefore, we consider in the following the limit $l_{\max} \rightarrow \infty$ in order to see that ν and $\bar{\nu}$ can be written as

$$\nu = \frac{1}{2}(\nu' + \nu'') \quad , \quad \bar{\nu} = \frac{1}{2}(\nu' - \nu'') , \quad (45)$$

where ν' and ν'' are two winding numbers defined w.r.t. two chiral Hamiltonians h'_k and h''_k which follow from the time evolution operators as

$$U_k(T, 0) = e^{-ih'_k T} \quad , \quad U_k(\frac{T}{2}, -\frac{T}{2}) = e^{-ih''_k T} . \quad (46)$$

Eq. (45) is the definition of $\nu_0 = \nu$ and $\nu_\pi = \bar{\nu}$ used in Ref. 3, where it was argued that these invariants define the number of TESs at energy $E = 0$ and $E = -\frac{\Omega}{2}$, respectively.

To prove (45) for an untruncated Floquet Hamiltonian we first define a convenient basis $\{|x_{k\sigma}^{\alpha r}\rangle\}$ in Floquet space, analog to (27)

$$h_k^F |x_{k\sigma}^{\alpha r}\rangle = \sigma(\epsilon_k^\alpha + r\Omega) |x_{k\sigma}^{\alpha r}\rangle \quad , \quad S_F |x_{k\sigma}^{\alpha r}\rangle = |x_{k\bar{\sigma}}^{\alpha r}\rangle , \quad (47)$$

$$\bar{h}_k^F |\bar{x}_{k\sigma}^{\alpha r}\rangle = \sigma(\bar{\epsilon}_k^\alpha + r\Omega) |\bar{x}_{k\sigma}^{\alpha r}\rangle \quad , \quad \bar{S}_F |\bar{x}_{k\sigma}^{\alpha r}\rangle = |\bar{x}_{k\bar{\sigma}}^{\alpha r}\rangle , \quad (48)$$

where $0 < \epsilon_k^\alpha, \bar{\epsilon}_k^\alpha \leq \frac{\Omega}{2}$, $\alpha = 1, \dots, d$, $\sigma = \pm$, $r = 0, \pm 1, \pm 2, \dots$, and

$$|x_{k\sigma}^{\alpha r}\rangle = T_{\bar{\sigma}r} |x_{k\sigma}^\alpha\rangle \quad , \quad |\bar{x}_{k\sigma}^{\alpha r}\rangle = T_{\bar{\sigma}r} |\bar{x}_{k\sigma}^\alpha\rangle , \quad (49)$$

together with $|x_{k\sigma}^\alpha\rangle = |x_{k\sigma}^{\alpha, r=0}\rangle$, $|\bar{x}_{k\sigma}^\alpha\rangle = |\bar{x}_{k\sigma}^{\alpha, r=0}\rangle$ and

$$\bar{\epsilon}_k^\alpha = -\epsilon_k^\alpha + \frac{\Omega}{2} \quad , \quad |\bar{x}_{k+}^\alpha\rangle = |x_{k-}^\alpha\rangle \quad , \quad |\bar{x}_{k-}^\alpha\rangle = T_1 |x_{k+}^\alpha\rangle . \quad (50)$$

Using (32), we can write for the integrands of the winding numbers in Eq. (44)

$$\text{Tr}(q_k^F)^\dagger dq_k^F = 2 \sum_{\alpha r} \langle x_{k+}^{\alpha r} | S_F | dx_{k+}^{\alpha r} \rangle \quad , \quad \text{Tr}(\bar{q}_k^F)^\dagger d\bar{q}_k^F = 2 \sum_{\alpha r} \langle \bar{x}_{k-}^{\alpha r} | \bar{S}_F | d\bar{x}_{k-}^{\alpha r} \rangle . \quad (51)$$

Inserting (43) and (49), and using (50), we find

$$\begin{aligned} \text{Tr}(q_k^F)^\dagger dq_k^F &= 2 \sum_{\alpha r} \langle x_{k+}^\alpha | T_r P T_{-r} S | dx_{k+}^\alpha \rangle = 2 \sum_{\alpha r} \sum_{l l'} \langle x_{k+, l}^\alpha | (T_r P T_{-r})_{l l'} S | dx_{k+, l'}^\alpha \rangle \\ &= 2 \sum_{\alpha r} \sum_{l l'} \delta_{l-r, -l'+r} \langle x_{k+, l}^\alpha | S | dx_{k+, l'}^\alpha \rangle = 2 \sum_{\alpha} \sum_{\substack{l l' \\ l+l' \text{ even}}} \langle x_{k+, l}^\alpha | S | dx_{k+, l'}^\alpha \rangle \\ &= \sum_{\alpha} \sum_{l l'} \left\{ 1 + (-1)^{l+l'} \right\} \langle x_{k+, l}^\alpha | S | dx_{k+, l'}^\alpha \rangle = \sum_{\alpha} \left\{ \langle y_{k+}^\alpha | S | dy_{k+}^\alpha \rangle + \langle \bar{y}_{k+}^\alpha | S | d\bar{y}_{k+}^\alpha \rangle \right\} , \end{aligned} \quad (52)$$

$$\begin{aligned} \text{Tr}(\bar{q}_k^F)^\dagger d\bar{q}_k^F &= 2 \sum_{\alpha r} \langle x_{k+}^\alpha | T_{-1} T_{-r} T_1 P T_r T_1 S | dx_{k+}^\alpha \rangle = 2 \sum_{\alpha r} \sum_{l l'} \langle x_{k+, l}^\alpha | (T_{-r} P T_{r+1})_{l l'} S | dx_{k+, l'}^\alpha \rangle \\ &= 2 \sum_{\alpha r} \sum_{l l'} \delta_{l+r, -l'-r-1} \langle x_{k+, l}^\alpha | S | dx_{k+, l'}^\alpha \rangle = 2 \sum_{\alpha} \sum_{\substack{l l' \\ l+l' \text{ odd}}} \langle x_{k+, l}^\alpha | S | dx_{k+, l'}^\alpha \rangle \\ &= \sum_{\alpha} \sum_{l l'} \left\{ 1 - (-1)^{l+l'} \right\} \langle x_{k+, l}^\alpha | S | dx_{k+, l'}^\alpha \rangle = \sum_{\alpha} \left\{ \langle y_{k+}^\alpha | S | dy_{k+}^\alpha \rangle - \langle \bar{y}_{k+}^\alpha | S | d\bar{y}_{k+}^\alpha \rangle \right\} , \end{aligned} \quad (53)$$

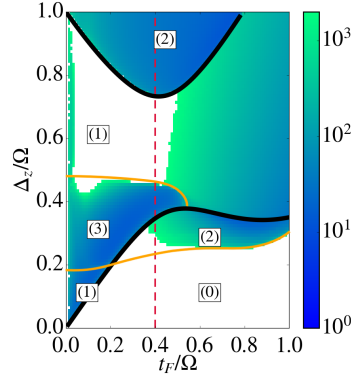


FIG. 1: Phase diagram for 3 Floquet replicas. The black (orange) phase boundaries indicate transitions where the number of TESs is changing by an odd (even) number (so-called type ‘‘A’’ (‘‘B’’) phase transitions). In each phase region the number of TESs is indicated in the boxes. The color indicates the localization length ξ of the strongest-localized TES. The regions are colored in white if no TESs are present or if $\xi > 2000$. The vertical dashed line indicates the value of t_F along which the position of the roots of $D_k^+ = \det A_k^+ = 0$ are shown in Fig. 2.

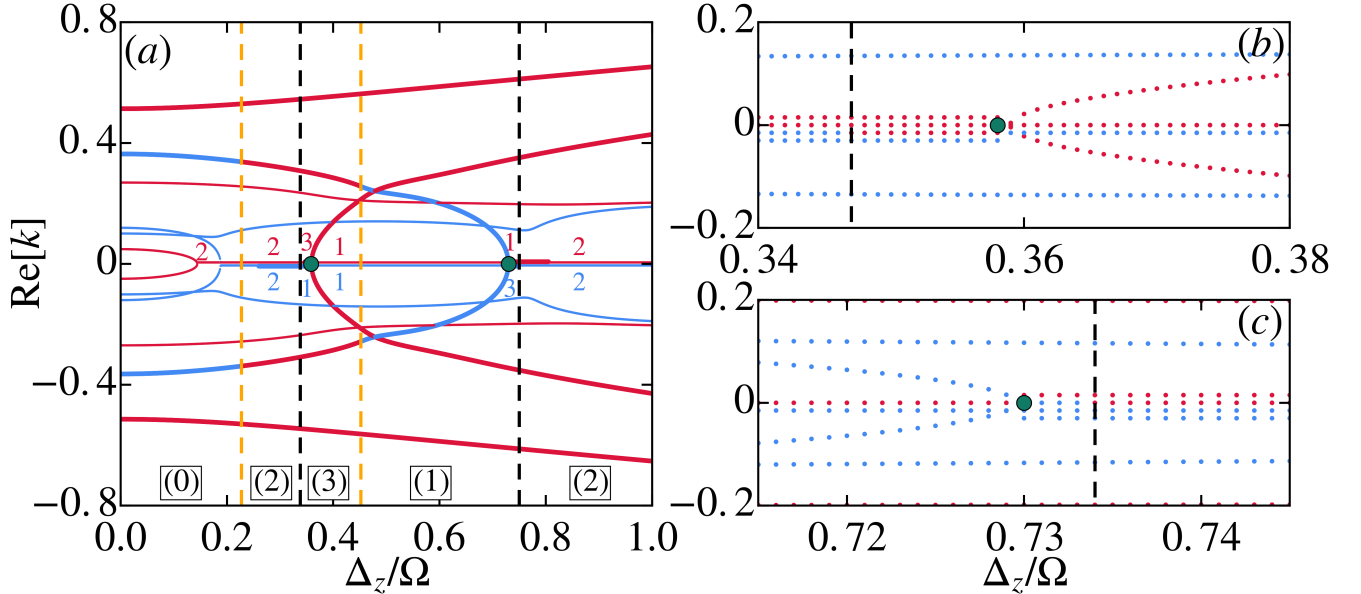


FIG. 2: The evolution of the real parts $\text{Re}(k_i)$ of the roots of $D_k^+ = \det A_k^+ = 0$ for 3 Floquet replicas as a function of Δ_Z at fixed $\frac{t_F}{\Omega} = 0.4$ (i.e., along the dashed line in Fig. 1). Blue/red lines correspond to roots with $\text{Im}(k_i) \geq 0$. The vertical dashed lines correspond to phase transitions of type ‘‘A’’ (black) or ‘‘B’’ (orange). The two transitions of type ‘‘A’’ are shown on a smaller scale in (b) and (c). If the real part of several roots is zero we indicate their number in (a) and use a slight offset in (b) and (c). Thick lines in (a) indicate roots with $|\text{Im}(k_i)| < 0.14$. The boxes in (a) contain the number of TESs in the various phases. The green dots indicate bifurcation points which are very close to the phase transitions.

where we have defined

$$|y_{k\sigma}^\alpha\rangle = \sum_l |x_{k\sigma,l}^\alpha\rangle = \sqrt{T} |x_{k\sigma}^\alpha(t=0)\rangle \quad , \quad |\tilde{y}_{k\sigma}^\alpha\rangle = \sum_l (-1)^l |x_{k\sigma,l}^\alpha\rangle = \sqrt{T} |x_{k\sigma}^\alpha(t=\frac{T}{2})\rangle. \quad (54)$$

As a result we find with (32) that Eq. (45) holds, where ν' and ν'' are the winding numbers of two Hamiltonians h'_k and h''_k , respectively, which have chiral symmetry S and are formally defined by

$$h'_k = \sum_{\alpha\sigma} \sigma \epsilon_k^\alpha |y_{k\sigma}^\alpha\rangle \langle y_{k\sigma}^\alpha| \quad , \quad h''_k = \sum_{\alpha\sigma} \sigma \epsilon_k^\alpha |\tilde{y}_{k\sigma}^\alpha\rangle \langle \tilde{y}_{k\sigma}^\alpha|. \quad (55)$$

These Hamiltonians are identical to the ones defined via (46) since due to (38) the time evolution operator can be

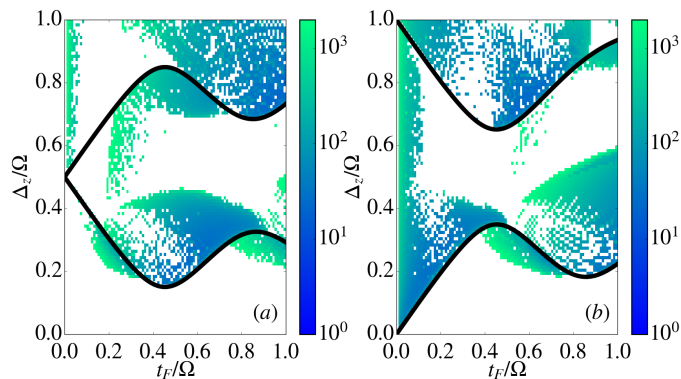


FIG. 3: Exact diagonalization study for the tight-binding Floquet Hamiltonians (a) $h_{nn'}^{e,3}$ (6 replicas) and (b) $h_{nn'}^{o,2}$ (5 replicas) on a finite system with $N = 10000$ unit cells. The parameters are $W = 8$, $\alpha = 0.3$ and $\Omega = 0.4$. The color indicates the localization length of the strongest-localized edge state. Only those edge states are considered which lie deeply in the bulk gap (within 15% away from the gap center relative to the bulk gap).

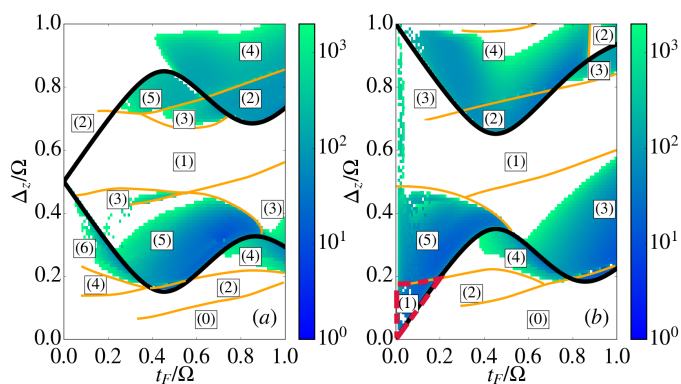


FIG. 4: Phase diagrams for the tight-binding Floquet Hamiltonians (a) $h_{nn'}^{e,3}$ (6 replicas) and (b) $h_{nn'}^{o,2}$ (5 replicas) on a half-infinite system (all other parameters as in Fig. 3).

written as

$$U_k(t, t') = T \sum_{\alpha\sigma} e^{-i\sigma\epsilon_k^\alpha(t-t')} |x_{k\sigma}^\alpha(t)\rangle \langle x_{k\sigma}^\alpha(t')|. \quad (56)$$

IV. TOPOLOGICAL PHASE DIAGRAM FOR 3 FLOQUET REPLICAS

In this section we consider the case of 3 Floquet replicas for the specific model considered in the main part of the paper¹. In Fig. 1 we show the topological phase diagram and relate it in Fig. 2 to the evolution of the real parts of the roots of $D_k^+ = \det A_k^+ = 0$ along the dashed line in Fig. 1. For higher truncation order the number of roots increases and the evolution of the roots becomes more complex. However, there are many roots with large imaginary part (the thin lines in Fig. 2(a)) which do not change the sign of their imaginary part and contribute only weakly to the TESs (if present). Therefore, they do not influence the number Z of TESs and do not participate in the phase transitions. The roots with imaginary part below a certain threshold (indicated by thick lines in Fig. 2) are the most important ones and are related to the local minima of the bulk band structure (shown in the main part of the paper for $\frac{\Delta_z}{\Omega} = 0.65$). As can be seen there are two phase transitions of type “B” (orange lines in Fig. 1 and orange dashed vertical lines in Fig. 2), where two roots with finite real parts at $\pm k_i$ simultaneously cross the real axis and change the sign of their imaginary part. According to (18) this changes the number Z of TES by two. In addition, there are two phase transitions of type “B” (black lines in Fig. 1 and black dashed vertical lines in Fig. 2), where only one root is crossing through $k = 0$ along the imaginary axis, which changes the number Z of TES by one. Both phase transitions of type “B” are associated with a bifurcation point lying very close to the phase transition (shown on a

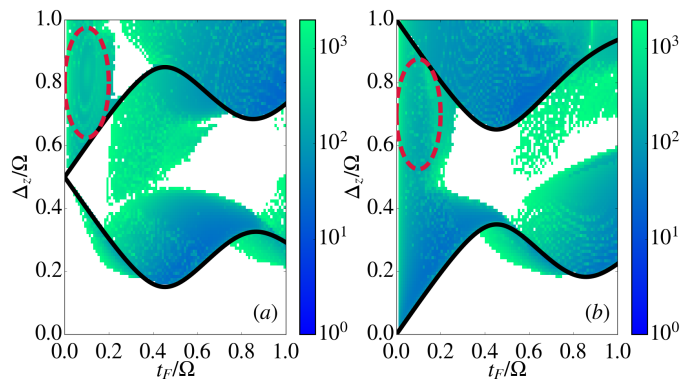


FIG. 5: Exact diagonalization study as in Fig. 3 but showing the strongest-localized edge state out of the first 20 eigenstates lying closest to the energy (a) $E = -\frac{\Omega}{2}$ and (b) $E = 0$. The regions where additional NTEs show up with very short localization length are indicated by red-dashed contours.

smaller scale in Fig. 2(b,c)).

V. EXACT DIAGONALIZATION STUDY AND NONTOPOLOGICAL EDGE STATES

In this section we present the results for the phase diagram of the specific model discussed in the main part of the paper¹ from an exact diagonalization study of the Hamiltonians $h_{nn'}^{e/o, l_{\max}}$ on a finite system with $N = 10000$ unit cells and discuss the occurrence of nontopological edge states (NTEs) at a finite energy distance from the gap centers.

Using exact diagonalization the results for the localization length of the strongest-localized TES are shown in Fig. 3. To identify the TESs and distinguish them from NTEs we consider only those edge states in this figure which lie very close to the energies $E = -\frac{\Omega}{2}$ and $E = 0$, i.e., very deep in the bulk gap. For a finite system, due to parity symmetry $U|n\sigma\eta l\rangle = |N - n + 1, -\sigma\eta l\rangle$ of the considered model (where n , σ , η , and l denote the indices for the unit cells, spin up/down, conduction/valence band, and Floquet modes, respectively), each TES will occur as a pair with parity \pm . The energy will not be exactly in the gap center since two edge states located only at the left/right end of the wire will have a small overlap leading to a small splitting in symmetric/antisymmetric TESs w.r.t. parity. This splitting is exponentially small and, therefore, the TESs are found in the exact diagonalization study from the states lying very close to the gap centers at $E = -\frac{\Omega}{2}$ or $E = 0$. Taking the criterium that the energy should lie within 15% of the bulk gap, the phase diagram for the localization length of the strongest-localized TES are roughly consistent with the results from the half-infinite wire shown in Fig. 4. There is still some noise visible in the exact diagonalization study since the criterium to find the TES deep in the bulk gap requires a precise determination of the bulk gap. This is often quite difficult since the bulk gap is dominated by very small gaps from anticrossings at large quasimomentum. In addition, one can also determine the number of TESs in each phase region from the exact diagonalization (not shown in Fig. 3) and finds a good agreement with Fig. 4. Only for small t_F numerical instabilities lead to very strong noise and a comparison is not possible.

To reveal NTEs at finite energy (either located in the gap or in the bulk spectrum), we have shown in Fig. 5 the localization length of the strongest-localized edge state out of the first 20 eigenstates lying closest to the center of the gap (for the same number of Floquet replicas as in Fig. 4). In comparison to Fig. 4 additional NTEs appear for $\Delta_Z \gtrsim \frac{\Omega}{2}$. Of particular interest are the ones with very short localization length and energies within the bulk gap which are indicated by a red dashed contour. These edge states are nondegenerate and can not stay in the bulk gap in the thermodynamic limit $N \rightarrow \infty$ since they have definite parity (only two degenerate edge states with different parities can be localized at the left or right end of the wire by a linear combination). They occur since the bulk gap is of $O(1/N)$ for small t_F determined from anticrossings with large quasimomentum. The bulk states at this anticrossing are discrete states with level spacing of the order of the gap. The NTEs are formed by a linear combination of an edge state from anticrossings with small quasimomentum and large gap (leading to a short localization length) with one of the discrete bulk states of the anticrossings with large quasimomentum and small gap. This pushes the NTEs slightly back into the bulk gap. However, for $N \rightarrow \infty$, the NTEs will not repel from a discrete bulk state but will be smeared out via a coupling to the continuum of states from the anticrossings at large quasimomentum with very small gap. This gives the NTEs a small broadening and its quasienergy will lie in the bulk. This is similar to broadening effects of TESs when anticrossings with small gap at large quasimomentum are closed by inelastic interactions. We note that, for small t_F , the NTEs indicated in the red-dashed contour of Fig. 5 have even a smaller localization length

compared to the TESs occurring in these phase regions. Therefore, they will also be observable in STM experiments but their energy is very unstable such that they can not be used for quantum computing operations.

In contrast, all other NTESs shown in Fig. 5 (not within the dashed contours) are NTESs lying already in the bulk spectrum. They have a very strong contribution from bulk states such that only a fraction of the particle is located at the edge. Nevertheless, the localization length calculated from the inverse participation ratio is rather small since both the edge and the bulk state forming a linear combination for the NTES are normalized wave functions leading to a very small prefactor $\sim 1/\sqrt{N}$ for the bulk contribution.

* Email: schoeller@physik.rwth-aachen.de

¹ D.M. Kennes, N. Müller, M. Pletyukhov, C. Weber, C. Bruder, F. Hassler, J. Klinovaja, and H. Schoeller, submitted to Phys. Rev. Lett.

² In preparation.

³ J.K. Asbóth, B. Tarasinski, and P. Delplace, Phys. Rev. B **90**, 125143 (2014).